Published Online First: September, 2024
https://doi.org/10.21123/bsj.2024.9359
P-ISSN: 2078-8665 - E-ISSN: 2411-7986
Baghdad Science Journal

Adsorption and Photocatalytic of Biosynthesis Zinc Ferrite Nanoparticles for Removing Acid Black 210 Dye from Aqueous Medium

Zahraa A. Najm [1], ***Mohammed A. Atiya**** [1], ***Ahmed K. Hassan*** [2]

[1] Department of Biochemical Engineering ,Al-Khwarizmi College of Engineering, University of Baghdad, Baghdad, Iraq.
[2]Environment and Water Directorate, Ministry of Science and Technology, Baghdad, Iraq.
*Corresponding Author.

Received 10/09/2023, Revised 07/01/2024, Accepted 09/01/2024, Published Online First 20/09/2024

Abstract

This study treated Acid black 210 dye contaminated textile wastewater by adsorption and photocatalytic techniques using zinc ferrite nanoparticles. Zinc ferrite nanoparticles were formed by the green synthesis technique using eucalyptus leaves as reducing and capping agents. SEM, EDAX, XRD, BET, Zeta potential, and FTIR techniques identified the resulting zinc ferrite nanoparticles. The images from the SEM indicated the crystallinity and spherical shape of the zinc ferrite nanoparticles with a particle size of 32 nm. In addition, this study involved using a photoreactor to accomplish the photo-degradation process. Effect of the main factors on the adsorption and photocatalytic degradation of dye was examined. Based on adsorption results, the removal efficacy of dye after 180 min was 74 % at optimum conditions of 5 mg/L, 0.75 g/L, 5, and 45 °C for AB210 concentration, Zinc ferrite nanoparticles dosage, pH, and temperature, respectively. In contrast, the photodegradation results show that five mg/L of dye was entirely removed within 30 min at optimal pH of 7, UV-intensity 24 W/m^2, and a temperature of 45 °C. The adsorption isotherms were studied using Freundlich, Langmuir, Temkin, and Dubinin models.

Keywords: Adsorption process, Green method, Kinetic and thermodynamic studies, Photocatalyst, Zinc ferrite nanoparticles.

Introduction

Dyes are an extensive group of pollutants found worldwide [1]. These dyes are primarily employed in a variety of industries, including cosmetics, textiles, rubber, and pharmaceuticals [2]. Substances utilized to prepare dyes are also extremely toxic or carcinogenic, posing numerous health concerns to people [3,4]. Several techniques have been documented to eliminate synthetic dyes, including filtration, coagulation, precipitation, ozonation, ion exchange, reverse osmosis, advanced oxidation, adsorption [5], and photocatalytic degradation processes have removed organic pollutants from polluted wastewater [6]. Adsorption has an advantage over other technologies due to its simple design and inexpensive investment in terms of initial cost and land. Adsorption is a technology frequently employed in industrial wastewater treatment to remove organic and inorganic impurities, and it has piqued the interest of researchers [7].

Photocatalytic degradation is an efficient technology for nonselective mineralization of dyes due to its convenience of use, low cost, and employment of highly reactive and powerful oxidative free radicals [8]. (AOPs), which involve the generation of hydroxyl free radicals (•OH), are considered promising [9]. The photocatalytic process is one of the AOPs that involves using semiconductors like (TiO_2) [10], (ZnS) [11], (ZnO) [12], and (Fe_2O_3) [13] to generate •OH and other

Published Online First: September, 2024
https://doi.org/10.21123/bsj.2024.9359
P-ISSN: 2078-8665 - E-ISSN: 2411-7986
Baghdad Science Journal

reactive oxidizing species. Both organic and inorganic contaminants can be destroyed by AOPs [6]. Between magnetic ferrites nanoparticles, zinc ferrite (ZnF-NPs) have gained attention in several fields, such as supercapacitors, gas sensors, hydrogen sensors, and photocatalytic applications [14].

Green metal nanoparticle synthesis has an advantage over other traditional chemical approaches since it is easy, safe, one-step, and inexpensive, reducing the risk of toxicity in our system, and developing stable, reproducible materials [15,16]. Plant extracts in general such as, Ficus leaves extract [17], for the synthesis of bimetallic Iron/copper nanoparticles, and tea leaves extract for the synthesis of Iron nanoparticles [18], bacterial or fungal biomass [19] and biopolymers are used to produce nanoparticles. The plant extract includes various aromatics and phenolic species, reducing metal salt and stabilizing the nanoparticles [20]. It is also environmentally friendly because it emits no toxic byproducts into the environment [21,22]. The mechanism proposed for the photocatalyst reaction in the presence of zinc ferrite is the potential of ZnF NPs to oxidize pollutants in the system, according to [23].

$$\mathbf{ZnFe_2O_4 + hv \rightarrow ZnFe_2O_4\ (e^-_{CB} + h^+_{VB})} \quad 1$$

Oxidation of water holes

$$\mathbf{h^+_{VB} + H_2O \rightarrow H^+ + \bullet OH} \quad 2$$

Oxidation of hydroxyl ions by hole

$$\mathbf{h^+_{VB} + OH \rightarrow \bullet OH} \quad 3$$

Oxygen reduction by electron

$$\mathbf{O_2 + e^- \rightarrow .^{\bullet}O_2^-} \quad 4$$

The dye's interaction with hydroxyl radicals

$$\text{Dye} + \mathbf{.^{\bullet}O_2^-} \rightarrow \text{products Degradation} \quad 5$$

$$\text{Dye} + \mathbf{h^+_{VB}} \rightarrow \text{products Degradation} \quad 6$$

$$\mathbf{.^{\bullet}O_2^- + HO_2^{\bullet} \rightarrow H^+ \rightarrow H_2O_2 + O_2} \quad 7$$

$$\text{Dye} + \mathbf{\bullet OH} \rightarrow \text{Degradation of the dye} \quad 8$$

There are no studies that have discussed the green method's ability, "especially eucalyptus leaves," to produce ZnF-NPs. Synthesis of ZnF-NPs by various extracts such as piper nigrum seeds [24], M.burkeana plant [25], and Limonia acidissima juice [26]. This study employed eucalyptus leaves extract as the green reducing and capping agent to generate ZnF-NPs.

This study's primary goal is to investigate the degradation of acid black 210 (AB210) dyes from the synthesis of aqueous solutions by two approaches (Adsorption and Photocatalytic processes) using a low-cost and eco-friendly catalyst as follows:

1- The green synthesis of zinc ferrite (ZnF-NPs) nanoparticles is environmentally friendly and prepared for the first time from eucalyptus leaves easily and economically. Eucalyptus trees are available locally and abundantly.

2- Using a photoreactor employing 24 UV-A lamps. It has a wavelength of 365 nm. It is located within the ultraviolet region (UV-A) of electromagnetic radiation, as most of the sun's rays that reach the earth are within the ultraviolet region (UV-A), and in the future, it is possible to rely on sunlight only as a source of energy as an alternative to using the photoreactor to investigate the degradation of the same dye (AB210) by the batch photocatalytic process.

Materials and Methods

Chemicals

The compounds used were of high purity (99.9%). Eucalyptus leaves used in this work were picked up from the garden of the University of Baghdad, Iraq. The dye acid black 210 (AB210) was taken from the leather tanning factory (Karadaa region). $Zn(NO_3)_2$ and $Fe(NO_3)_3$ were obtained from a central drug house (CDH) in India, while 100% ethanol was obtained from CARLO ERBA reagents in France.

Catalyst Preparation

1- Preparation of the leaf extract

The synthesis procedure was taken from [6] with slight modifications. Initially, the eucalyptus leaves were picked up from the yard at the University of Baghdad and repeatedly washed for dust and difficult dirt removal using distilled water. The leaves were then dried in the oven for 12 hours at 50 centigrade. The leaves were crushed to a fine powder when thoroughly dried. 150 mL of deionized water was used to wet 10 g of powdered eucalyptus leaves in an Erlenmeyer flask for 30 minutes while stirring at 80°C. The resulting extract was cooled and filtered through filter paper; the filtrate was then kept at four centigrade before it was used as a capping and

Published Online First: September, 2024
https://doi.org/10.21123/bsj.2024.9359
P-ISSN: 2078-8665 - E-ISSN: 2411-7986
Baghdad Science Journal

reducing agent to synthesis zinc ferrite nanoparticles (ZnF-NPs).

2- To complete the ZnF-NPs preparation, zinc nitrate of 2.273 g and ferric nitrate of 7.23 g were submerged in 100 mL of deionized water. Following that, 150 mL of eucalyptus leaves extract (reducing agent) was slowly added to the salts solution with agitated for approximately 60 minutes. The produced solution was microwaved for 15 minutes in a domestic microwave oven. Following that, mixture was vacuum filtered and rinsed with distilled water many times and 100% pure ethanol. The collected black precipitate was calcined at 600 centigrade for 4 hours before being pulverized with a mortar and pestle to a fine powder See Fig. 1 [26].

Several characterization techniques were applied to analyze the synthesized ZnF-NPs to characterize the structure, morphology, specific surface area, size, and other essential characteristics. The size and shape were identified using SEM (model Tescan Vega3, USA). The latter is paired with an EDAX examination that provides more details regarding the chemical components. Additionally, specific surface area, pore size, and pore volume were determined using the BET analysis (TriStar II Plus version 2.03 instrument, USA). Finally, FTIR used for examine the functional groups of ZnF nanoparticles (Shimadzu, Japan).

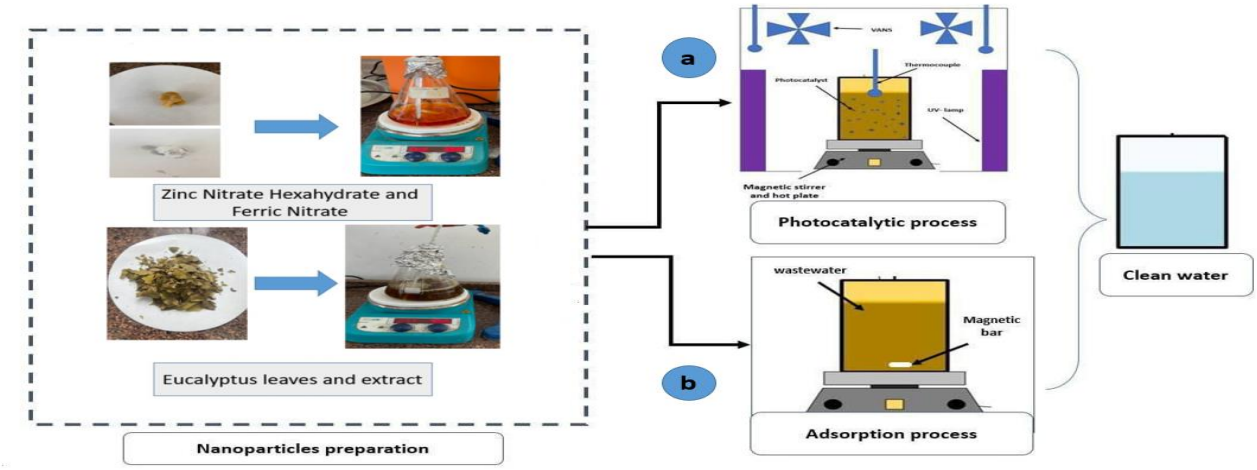

Figure 1. Schematic diagram of ZnF-NPs Synthesis, (a) Photocatalytic process in Photoreactor, (b) Adsorption process

Batch Process

Batch experiments of AB210 removal through an adsorption and photocatalytic process were carried out in a Beaker Pyrex 1 liter. The effect of several operational parameters was studied during both processes, including pH ranging (2-9), the temperature ranging (25-55 ℃), AB210 concentration ranging from (5- 40 mg/L) and amount of ZnF-NPs in the range of (0.1-1 g/L). Initially, (One M from H_2SO_4 and NaOH) were utilized to modify the pH of solutions. Accordingly, in adsorption process ZnF-NPs were added to the dye solution and magnetically shaken for 2 minutes and at a temperature of 25 ℃ to enable the ZnF-NPs to be diffused homogeneously inside the solution. The ZnF-NPs Synthesis and using in two adsorption and photocatalytic process using a photoreactor, The photoreactor is used to accomplish the photocatalysis process under UV- light radiation type A. 24 UV-A lamps, at a maximum wavelength peak of 365 nm were put within a cylindrical aluminium container to create a reflecting surface for incident photons. The photo reactor has two fans installed at the top that supplies cooling air and protects the reaction vessel from the hot lamps as shown in Fig. 2[27]. The samples were obtained at regular intervals during the experiment and filtered using a 0.45 µm membrane filter. Finally, A UV/Vis spectrophotometer with a max of 465nm was used to measure the concentration of AB210. Follows the equation was used to compute the AB210 removal efficiency.

$$\%DR = \frac{C_o - C_t}{C_o} x\ 100\ \% \qquad 9$$

Where %DR is the removal efficiency, $C_\bullet$ is initial AB210 (mg/L) and final C_t is AB210 at time t.

Published Online First: September, 2024
https://doi.org/10.21123/bsj.2024.9359
P-ISSN: 2078-8665 - E-ISSN: 2411-7986
Baghdad Science Journal

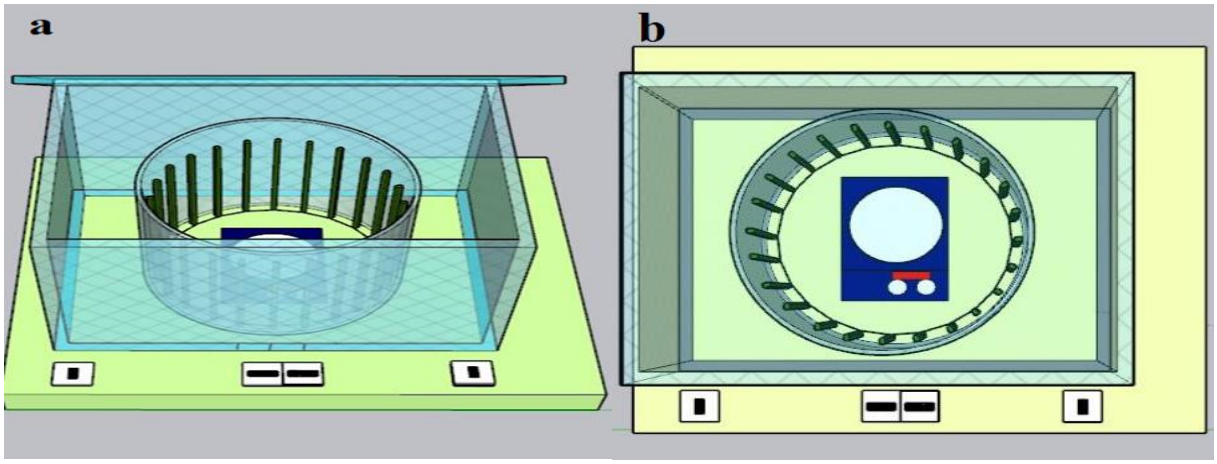

Figure 2. (a) Configuration of photoreactor used in the photocatalytic reaction, (b) top view of photoreactor.

Results and Discussion

Characterization of ZnF-NPs

FT-IR used a mid-IR spectrum (400-4000 cm^{-1}) to define functional groups of ZnF-NPs. Because of the O-H stretching of polyphenols, significant eucalyptus leaves extract peaks exhibited a broad band at 3419.79 cm^{-1} [28]. The spectrum depicts the two primary absorption peaks of spinel ferrite as shown in Fig. 3. The intrinsic stretching vibration of Zn-O at tetrahedral sites caused the strongest absorption band at 551.64 cm^{-1} [29]. The stretching vibration of Fe-O at octahedral sites caused the weakest absorption band at 441.70 cm^{-1}. The stretching vibration of the C-H bond is visible in the weak bands at 2924 and 1386 cm^{-1}. The H-O-H stretching vibration of adsorbed water molecules is ascribed to the band at 1641 cm^{-1}.The peak at 1031.92 cm^{-1} is attributed to carbon dioxide adsorbing on the particles' surface [30]. The results show that the prepared sample has the predicted ferrite structure.

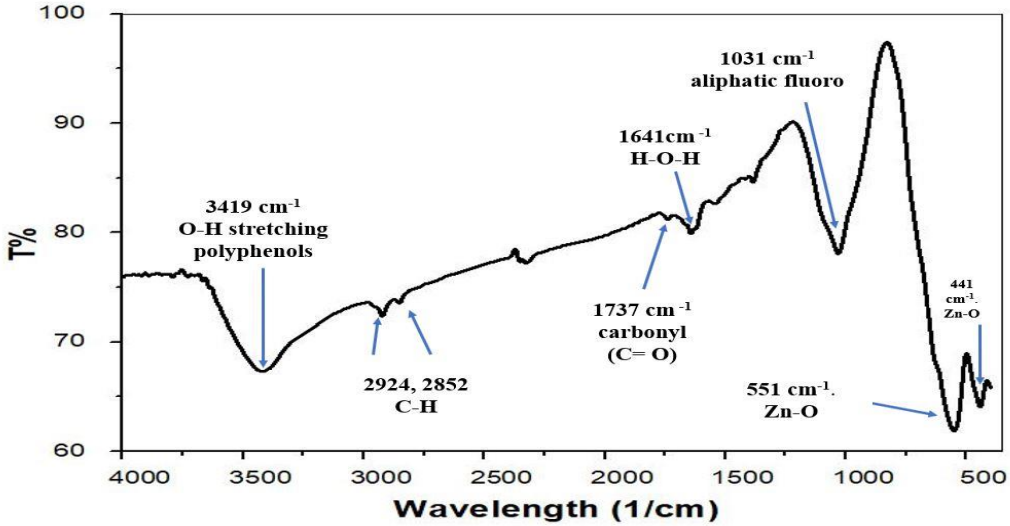

Figure 3. FT-IR of ZnF-NPs.

The estimated optical energy band gap was 2.52 eV as shown in Fig. 4. This discovery demonstrates that these $ZnFe_2O_4$ nanoparticles have a narrow bandgap, allowing them to function as an effective light catalyst. The fundamental process of photocatalyst activation. To do this, photons with energies (=hv) more significant than a photocatalyst's band gap (BG) must be absorbed [31]. This causes electrons (e^-) to move from the valence band to the conduction band, creating a hole (h^+) in the valence band. These

Published Online First: September, 2024
https://doi.org/10.21123/bsj.2024.9359
P-ISSN: 2078-8665 - E-ISSN: 2411-7986
Baghdad Science Journal

divided holes and electrons can, however, these separated holes and electrons can recombine and release the absorbed energy as heat. This photogenerated (e^-) and (h^+) then react with easily accessible oxidants and reductants to form powerful and unstable radicals, which react with the contaminant and mineralize it to carbon dioxide and water while also producing a variety of intermediary species See Fig. 5 [32].

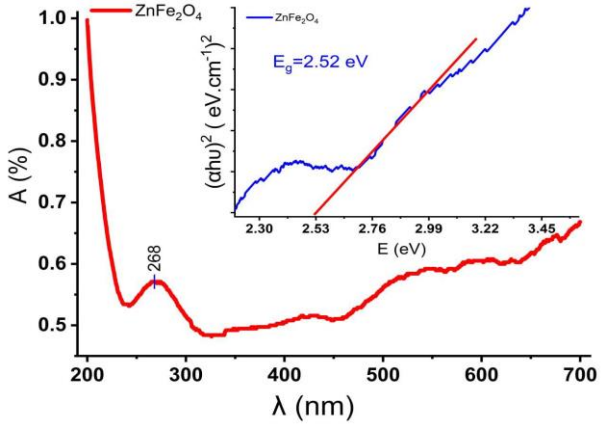

Figure 4. UV-Visible absorption spectra and band gap energy diagram of ZnF-NPs.

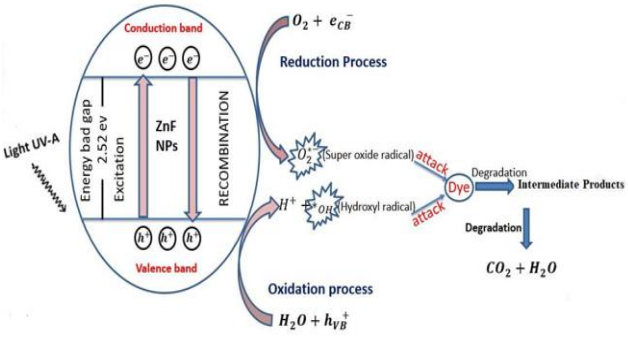

Figure 5. Basic principle of photo catalysis.

SEM of ZnF-NPs were taken at different magnifications of 1 µm, 500, and 200nm. High-magnification micrographs confirm the formation of ZnF-NPs with a mean diameter of 32 nm. Furthermore, aggregation was observed in some areas, which depended on the nature of the synthetic route and the radiation treatment used during the ZnF-NPs synthesis[33]. From these results, The $ZnFe_2O_4$ nanoparticles showed a homogeneously dispersed and narrow size distribution as shown in Fig. 6. EDAX analysis revealed the chemical compositions (Zn, Fe, and O) of produced nanoparticles as shown in Fig. 7. According to the figure, there are no impurities in the synthesized ZnF –NPs [34].

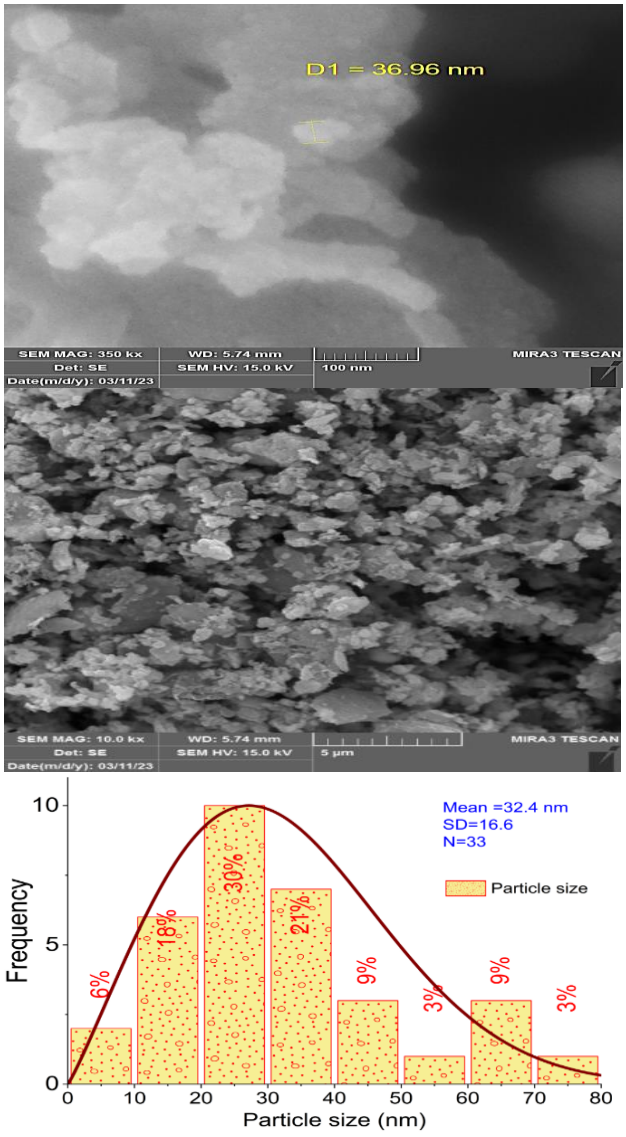

Figure 6. SEM of ZnF-NPs.

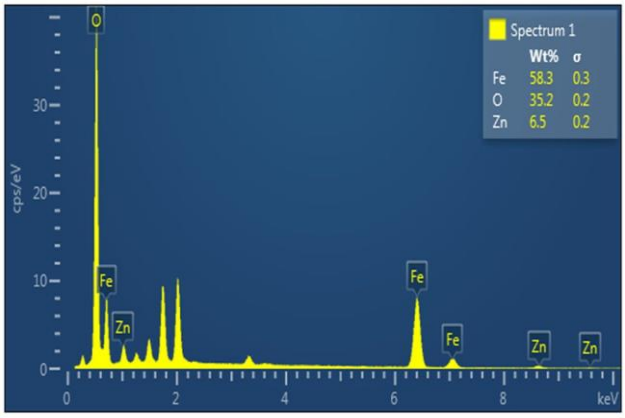

Figure 7. EDAX analysis of ZnF-NPs.

The pore size, (SSA), and pore volume were estimated using the (BET). The SSA, pore volume,

Published Online First: September, 2024
https://doi.org/10.21123/bsj.2024.9359
P-ISSN: 2078-8665 - E-ISSN: 2411-7986
Baghdad Science Journal

and pore size were 42 m^2/g, 0.11 cm^3/g, and 10 nm. Intervals between homogeneous metal-oxide and water molecule adsorption on the surface of the materials resulted in typical mesoporous structure [35]. The high SSA of ZnF NPs increases the efficiency of the adsorption and photocatalytic processes.

Zeta potential measurement is an essential indicator for determining particle stability. High zeta potential values indicate that the nanoparticles are stable and resist aggregation, whereas low potential indicates that the nanoparticles are unstable and have a high tendency to flocculate. That zeta potential analysis generated a high negative value of -47.41 mV, indicating that ZnF-NPs are stable as shown in Fig. 8 [36]. The presence of phenolic chemicals in eucalyptus leaf extract accounts for this stability [37,38].

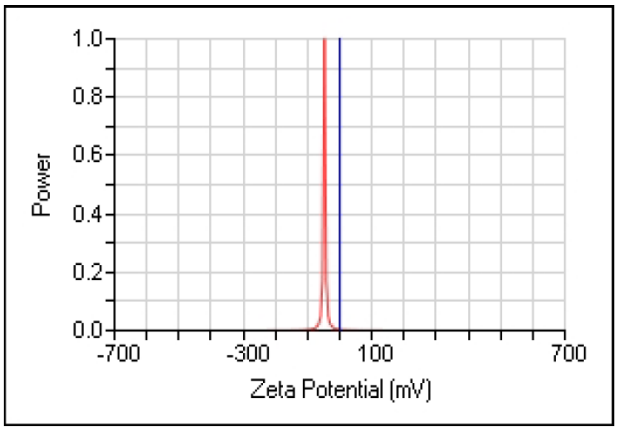

Figure 8. Zeta potential analysis of ZnF-NPs.

The XRD analysis was conducted to learn more about crystallinity, phase identification, and crystalline size, green synthesized $ZnFe_2O_4$ NPs calcined at 600°C displayed two diffraction peaks at 35.26, 46.86, 53.11, and 56.62, respectively, which are indexed to the planes (311), (331), (422), and (511). These peaks indicated that the cubic spinel structures of the ZnF-NPs had formed. The XRD patterns revealed that the peaks were extremely intense and narrow, indicating that the materials are highly crystalline. Other peaks, 2θ of 24.138, 33.152, 40.854, and 63.989 corresponding to (012), (104), (113), and (300), respectively as shown in Fig. 9, were identified as being related to the phase of hematite (α-Fe_2O_3). These peaks were identified as a result of the production of the hematite phase by air heating of spinel ferrites [39].

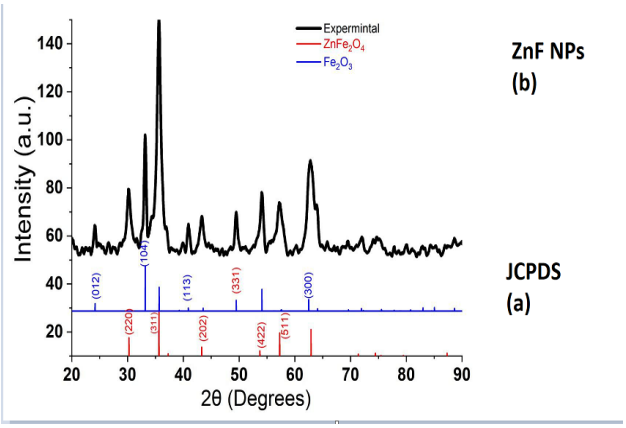

Figure 9. XRD patterns of synthesized ZnF nanoparticles (a) Standard XRD pattern and (b) ZnF NPs XRD pattern.

Effect of Parameters on Adsorption and Photocatalytic Process

Effect of the ZnF-NPs

The influence of ZnF-NPs dose on the degradation of AB210 was investigated, and the nanoparticle dose was adjusted between (0.1 -1 g/L) while the other operational conditions remained unchanged. Figure 10a illustrates the removal efficiency of AB210 after 300 min of adsorption experiments are 16,19,23, and 25 % for doses 0.1,0.25,0.5,0.75, and 1.0 g/L, respectively. Raising the adsorbent dosage, as indicated, improves the surface and availability of adsorption sites [40]. After reaching equilibrium, increasing the adsorbent dose reduces the extent of the AB210 removal capacity due to a split in flux or gradient of the concentrate between the concentration of the dissolved mass in the solution and the concentration of the dissolved mass in the adsorbent. When a result, once adsorbent mass increases, the amount of dye absorbed in the solution for each unit mass of adsorbent decreases [41]. In contrast, photo-degradation process, Fig. 10b illustrates the removal efficiency was 36, 50, 65, 68, and 71 % after 180 minutes for the same doses in adsorption experiments. These results showed that the photo-degradation rate increased with increasing catalyst loading. This phenomenon happened as a result of increased active surface area and the number of reaction sites. The preliminary promotion of higher degrading activity was related to enhance the photocatalyst's surface area, increased binding sites on the photocatalyst surface, and production of •OH [42] From an economic standpoint, 0.75 g/L ZnF-NPs was chosen as the optimum amount for both processes due to the highest removal efficiency when the ZnF-NPs amount was chosen to be the ideal

Published Online First: September, 2024
https://doi.org/10.21123/bsj.2024.9359
P-ISSN: 2078-8665 - E-ISSN: 2411-7986
Baghdad Science Journal

quantity for both processes due to the closest removal efficiency at 1 g/L of ZnF-NPs.

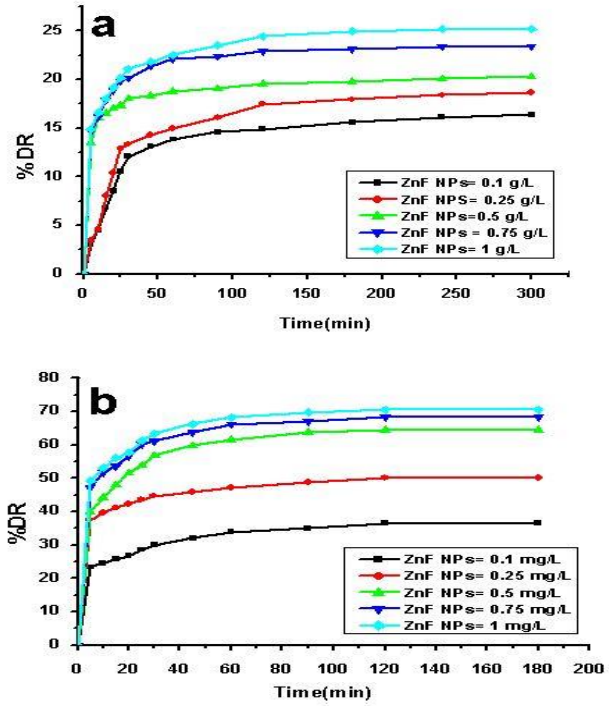

Figure 10. Effect of the amount of ZnF-NPs at AB210 concentration, pH, and temperature of 25 mg/L, 4 (a) 5 (b) and 25 ℃ respectively, (a) adsorption process, (b) photocatalytic process.

Effect of pH

The adsorbent charge's surface and solubility properties are controlled by how acidic, neutral, or essential the working solution, which substantially influences dye removal. Fig. 11a, shows that removal rate of AB210 was studied at pH range (2-9) by keeping other operating conditions constant. The AB210 removal efficiencies were 17, 20, 23, 39, 35, and 30 % for pH 2, 3, 4, 5, 7, and 9, respectively. Because ZnF-NPs partially dissolve at low pH (2 and 3), active sites on catalyst surface are diminished and thus reducing the removal efficacy of ZnF-NPs. Furthermore, at the essential condition (pH 9), the hydroxyl ion and AB210 molecules compete on the ZnF-NPs active sites, decreasing the removal efficiency [43,44].

Moreover, as in Fig. 11b, in the photo-degradation process, the AB210 removal rates increased from 42 to 75 % when pH increased from 2 to 7 and increased to 78 % at pH 9. This happened because the acidic media caused the photo-corrosion of ZnF-NPs, which led to the dissolution of the catalyst. In contrast, increasing the effectiveness of catalyst at primary conditions is due to the existence of more hydroxyl ions which facilitate the photo generation of hydroxyl radicals and prevent the dissolution of ZnF-NPs. As a result, 5 and 7 were selected as the ideal pH for the adsorption and photocatalysis processes, respectively.

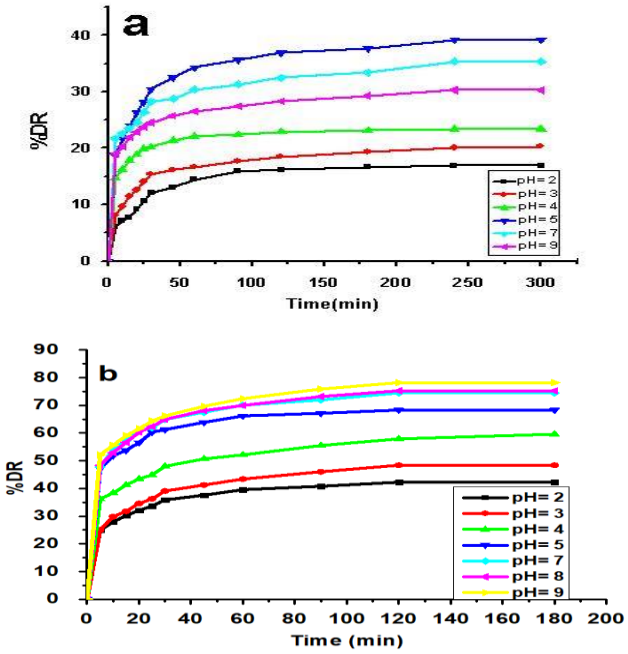

Figure 11. Effect of initial pH at ZnF-NPs dose, AB210 concentration, and temperature were 0.75 g/L, 25 mg/L, and 25 ℃, (a) adsorption process, (b) photocatalytic process.

The Effect of Temperature

By retaining all the other operation conditions constant, the temperature of experiments was changed in range (35-55 ℃). In Fig.12a, the adsorption process, the removal efficiencies of AB210 were 39% to 67 % when the temperature was raised from 25 to 55 ℃. With increasing temperatures, more active sites become available, and the adsorbent surface becomes activated, explaining the increase in the removal of AB210. In addition, the dye molecules obtained the necessary energy at higher temperatures because of enhanced diffusion and mobility of AB210 dye ions from the bulk solution to the surface of ZnF-NPs [45,46]. Figure 12b indicates that during the photodegradation process, the removal rate of AB210 was 75, 77, 81, and 83 % at a temperature of 25, 35, 45, and 55 ℃ after 180 minutes of photocatalytic reaction. Increasing temperature leads to faster photocatalytic reaction, increasing the production of •OH [47].

Published Online First: September, 2024
https://doi.org/10.21123/bsj.2024.9359
P-ISSN: 2078-8665 - E-ISSN: 2411-7986
Baghdad Science Journal

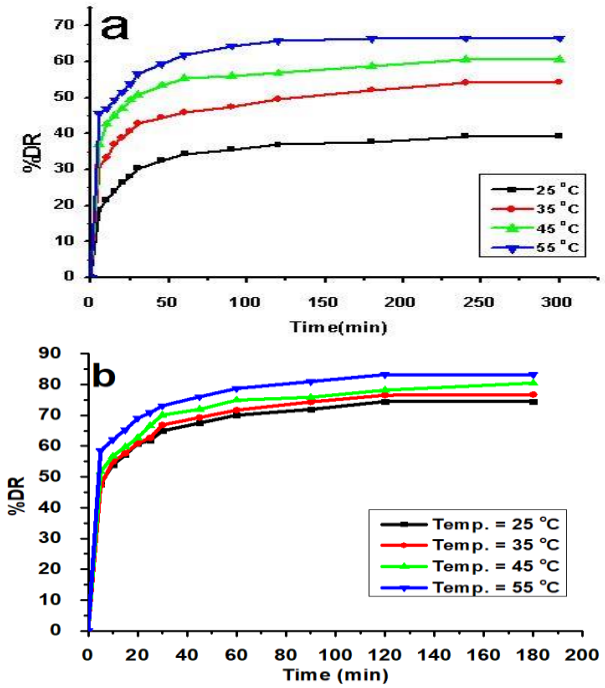

Figure 12. Effect of temperature at ZnF-NPs dose, concentration AB210, and pH were 0.75 g/L,25 mg/L, and 5 (a),7 (b) respectively, (a) adsorption process (b) photocatalytic process.

The Effect of UV Intensity

Fig. 13 illustrates the removal rate of AB210 was 72, 81, and 90% for UV intensity 6, 15 and 24 W/m^2, respectively. The removing efficacy enhanced as the UV intensity increased because it generated more photons, causing more electron-hole pairs to be excited and generating more •OH [48]. The UV intensity of 24 W/m^2 was regarded the best.

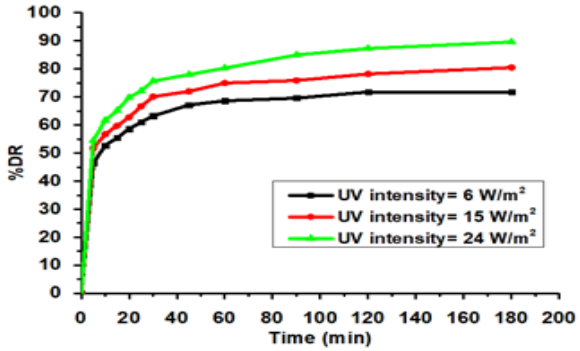

Figure 13. Effect of UV-intensity on photocatalytic process at ZnF-NPs dose, concentration AB210, pH, and temperature were 0.75 g/L, 25 mg/L, 7 and 45°C respectively.

The Effect of Initial AB210 Concentration

Initial concentration is a vital factor to study because it considered a driving force to force up the movement between the liquid and solid phases. As a result, the effects of AB210 removal efficiency were studied at AB210 concentration range from 5-40 mg/L while keeping the other operation conditions at optimum values. In Fig. 14a, the removal rates were 74, 66, 62, 44, and 39% at AB210 concentrations of 5-40 mg/L. The results showed that maximum removal were at 5 and 10 mg/L because unoccupied sites were available. Rising AB210 concentration of more than 10 mg/L causes more dyes molecules to go toward these open nanoparticle locations then the amount of accessible active sites in the adsorbent decreases, resulting in a reduced AB210 removal efficiency [9]. On the other side, Fig. 14b illustrates the photocatalytic degradation in the same range of dye concentration given removal efficiency of 100, 98.7, 94, 89.6, 85 and 81 % at AB210 concentrations of 5-40 mg/L, respectively. Beer-Lambert's law states that light absorption rises with dye concentration, preventing more photons, particularly in the deeper part of the solution, from reaching the catalyst surface. Therefore, the number of charge carriers produced and the degradation efficiency would decline, leading to decreased •OH production and, consequently, the removal efficiency [49,50]. Furthermore, the availability of active sites is a priority in the photocatalytic process, and increasing the initial AB210 concentration reduces the number of available active sites [51,52].

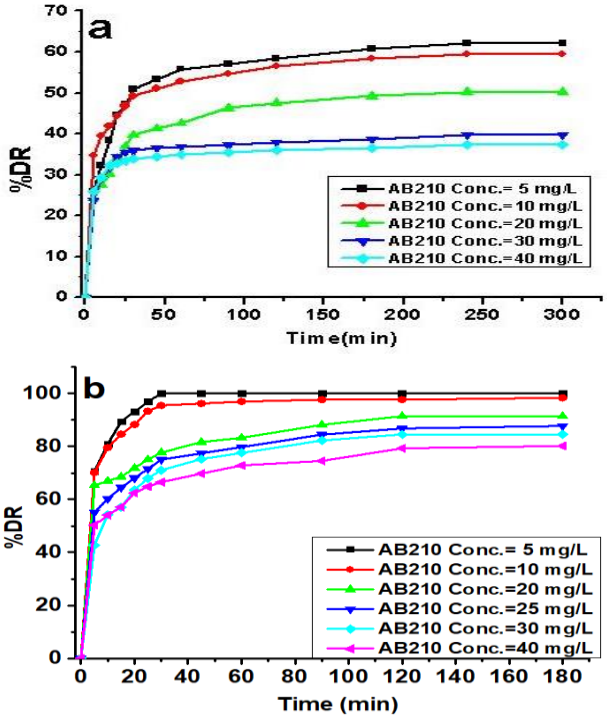

Figure 14. Effect of initial concentration AB210 at ZnF-NPs dose, pH, and temperature were 0.75

Published Online First: September, 2024
https://doi.org/10.21123/bsj.2024.9359
P-ISSN: 2078-8665 - E-ISSN: 2411-7986
Baghdad Science Journal

g/L, 5 (a) and 7 (b) 24 W/m^2 and 45 °C respectively, (a) adsorption process (b) photocatalytic process.

Adsorption Kinetics

To examine mechanism of dye sorption onto ZnF-NPs, the adsorption data was estimated using three models below. The following is the pseudo-first-order rate equation:

$$\log(q_e - q_t) = \log q_e - \frac{k_1 t}{2.303} \qquad 10$$

Where q_e and q_t are the dye-adsorbed amounts (mg/g) at equilibrium and t time (min), respectively, and k_1 (min $^{-1}$) is the pseudo-first-order rate constant. The values of k_1 were calculated from log (q_e – q_t) versus t plots, Fig. 15 a.

The rate equation for the pseudo-second-order model is as follows:

$$\frac{t}{q_t} = \frac{1}{k_2\, q_e^2} + \frac{t}{q_{eTo}} \qquad 11$$

Where k_2 (g/mg.min) is the pseudo-second-order rate constant derived from plots of t/q_t versus t Fig. 15 b.

Rate equation for the Elovich model is as follows:

$$q_t = \frac{1}{\beta}\ln(\alpha\beta) + \frac{1}{\beta}\ln(t) \qquad 12$$

Where: α initial adsorption rate (mg.[g. min]$^{-1}$), β : desorption rate constant (g.mg^{-1})

Table 1 demonstrates that the regression coefficient R^2 for the Elovich model was low, indicating poor model fit. In contrast, the regression coefficient R^2 for the pseudo-second-order kinetic model is greater than R^2 for the pseudo-first-order kinetic model, showing that the pseudo-second-order is the best-fit model to

represent AB210 adsorption kinetic by ZnF-NPs. Furthermore, the Elovich model is appropriate in chemical adsorption studies for systems with heterogeneous adsorbing surfaces. The slope and intercept between q_tand ln (t) can be used to get the Elovich parameters and, as illustrated in Fig. 15c, where and are the adsorption and desorption rate constants. Table 1 shows that changing the starting concentration of AB210 has an effect on the values of α and β. As a result, the value of β decreased as the initial AB210 concentration climbed from 5 to 40 mg/L, and there was no significant fluctuation with. Furthermore, the results demonstrated that the rate of adsorption α is greater than the desorption constant β, demonstrating the viability of adsorption.

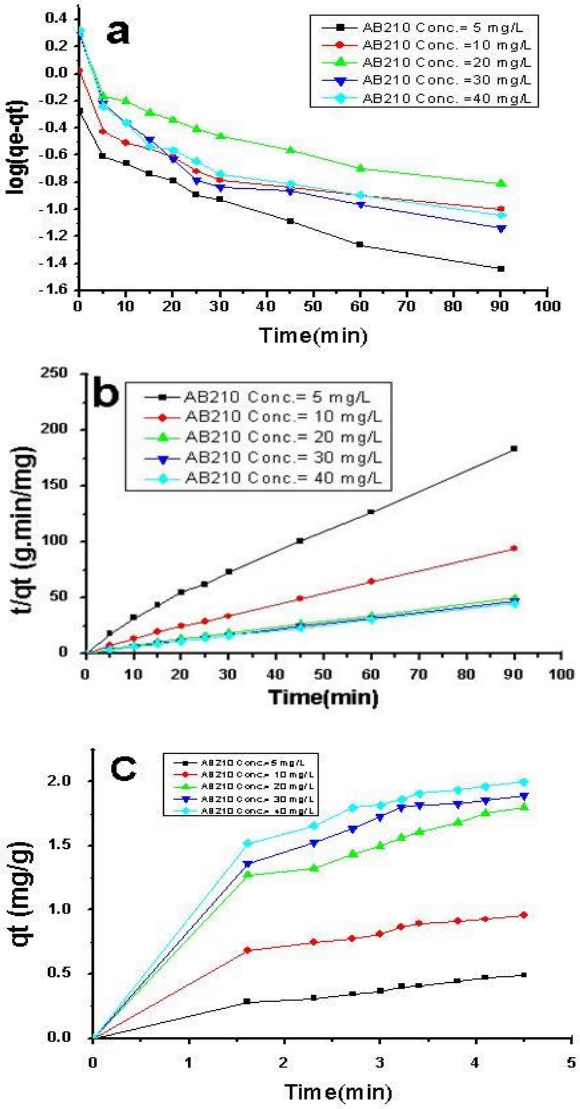

Figure 15. Kinetic models (a) pseudo-first-order, (b) pseudo-second-order, and (c) Elovich model.

Table 1. Adsorption kinetic parameters of AB210 onto ZnF-NPs.

AB210	Pseudo-first-order		Pseudo-second-order		Elovich model		
mg/L	k_1	R^2	k_2	R^2	α	β	R^2
5	0.0264	0.91	0.356	0.992	0.172	9.551	0.9
10	0.02	0.7	0.389	0.998	0.530	5.102	0.85
20	0.0225	0.78	0.167	0.997	0.932	2.717	0.87
30	0.0292	0.71	0.286	0.999	1.153	2.549	0.83
40	0.0267	0.69	0.197	0.998	1.346	2.465	0.8

Published Online First: September, 2024
https://doi.org/10.21123/bsj.2024.9359
P-ISSN: 2078-8665 - E-ISSN: 2411-7986
Baghdad Science Journal

Adsorption Thermodynamic

AB210 adsorption onto ZnF-NPs was studied at different temperatures (20, 35, 45, 55 ℃) to establish the adsorption's spontaneity, nature, and application. These adsorption qualities can be determined using (ΔG°), (ΔH°), and (ΔS°) thermodynamic parameters, which were obtained from the equations below[38].

$$\Delta G^o = \Delta H^o - T\Delta S^o \dots\dots 13$$
$$\Delta G^o = -RT\ln K_c \dots\dots 14$$
$$K_c = \frac{q_e}{C_e} \dots\dots 15$$

K_C is the distribution constant (L.g^{-1}). Similarly, Fig. 16a, ΔS° and ΔH° can be calculated from the intercept and slope of the graph of ΔG° vs temperature (K).

In addition, the Arrhenius equation described below can also be used to calculate activation energy.

$$\ln k_{obs} = \ln A - \frac{E_a}{RT} \quad 16$$

$$\ln\left(\frac{C_t}{C_o}\right) = -k_{obs}\, t \quad 17$$

Where E_a is the activation energy (kJ.mol^{-1}), *A* is the Arrhenius constant (J.mol^{-1}k^{-1}), and k_{obs} are the rate constant (min^{-1}). Fig. 16b illustrates the slope of the plot between ln (k_{obs}) and 1/T as represented by activation energy *Ea*. Table 2 illustrates the thermodynamic characteristics of the AB210 adsorption onto ZnF-NPs. At the investigated optimum temperature, the Gibbs free energy (ΔG°) was -1.895 kJ/mol, which had a positive value demonstrating the non-spontaneity of the adsorption process [53]. The positive value for ΔH° (30.5 kJ.mol^{-1}) revealed the adsorption of AB210 onto ZnF-NPs was an endothermic process at the solid-solution interface and that the AB210 ions had an appropriate affinity for nanoparticles. The result of (Δ*S*°) was positive (0.10173 kJ. mol.k^{-1}), showing increased spontaneous interference in the process of adsorption at the solid-liquid interface and a suitable affinity of AB210 ions for nanoparticles [54].

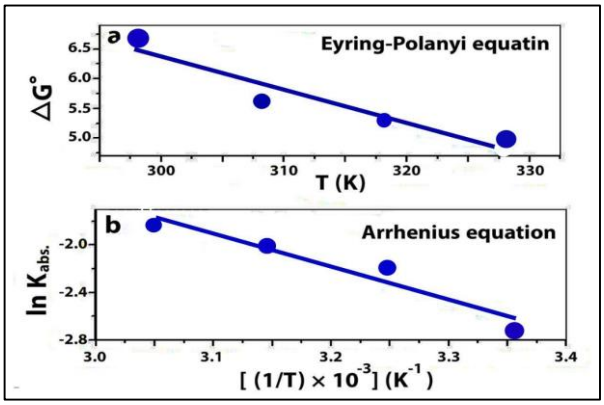

Figure 16. Linear form of (a) Eyring Polanyi equation, (b) Arrhenius equation for ZnF-NPs.

Adsorption Isotherm

The adsorption isotherm frequently calculates the maximum adsorption rate of adsorbates and adsorbents. The formulas (17-20) are utilized to analyze interaction between ZnF-NPs (the adsorbent) and AB210 (the adsorbed dye) in Langmuir, Temkin, Freundlich, and Dubinin isotherm model as illustrate in Fig. 17. Table .3 lists adsorption isotherm parameters.

Langmuir model is based on forming of a monomolecular adsorbate layer on the adsorbent's surface, and all active centers have the same energy and enthalpy. The equation for the Langmuir adsorption isotherm is as follows:

$$\frac{1}{q_e} = \frac{1}{q_{max}.K_L}\left(\frac{1}{C_e}\right) + \frac{1}{q_{max}} \quad 18$$

Where q_{max}: saturation adsorption of Langmuir (mg.L^{-1}) , K_L: equilibrium constant of Langmuir (L.mg^{-1}).

The Freundlich model is employed to illustrate adsorption on a heterogeneous surface. Due to this model, the adsorption centers have different energy values, and the active adsorption centers with the highest energy fill first. The Freundlich model isotherm equation appears as follows:

$$\log q_e = \left(\frac{1}{n}\right)\log C_e + \log K_F \quad 19$$

Where K_F: the Freundlich adsorption constants; $1/n$: factor of heterogeneity

According to the Temkin isotherm, the highest binding heat of sorption B_T was positive (0.5651 kJ.mol^{-1}), which denotes an exothermic adsorption process, Temkin model is shown below.

$$q_e = B_T \ln C_e + B_T \ln K_T \quad 20$$

Published Online First: September, 2024
https://doi.org/10.21123/bsj.2024.9359
P-ISSN: 2078-8665 - E-ISSN: 2411-7986
Baghdad Science Journal

$$B_T = \frac{RT}{b_T} \qquad 21$$

Where K_T: maximum binding energy (L.g^{-1}), B_T: maximum binding heat of sorption (KJ.mol^{-1}), R: ideal gas constant (0.008314 Kj.mol^{-1}.K^{-1}) ,and T: absolute temperature (K). Because it does not indicate surface homogeneity or adsorption potential constancy, the Dubinin isotherm is more general than the Langmuir isotherm.

$$nq_e = \ln q_m - \beta\varepsilon^2 \qquad 22$$

$$\varepsilon = RT \ln(1 + \frac{1}{C_e}) \qquad 23$$

$$E = \frac{1}{\sqrt{(2\beta)}} \qquad 24$$

Where q_m: the theoretical saturation capacity, β: Dubinin constant (mol^2 .Kj^{-2}) , ε: Duninin isotherm constant ,and E: adsorption energy (kJ.mol^{-1}).

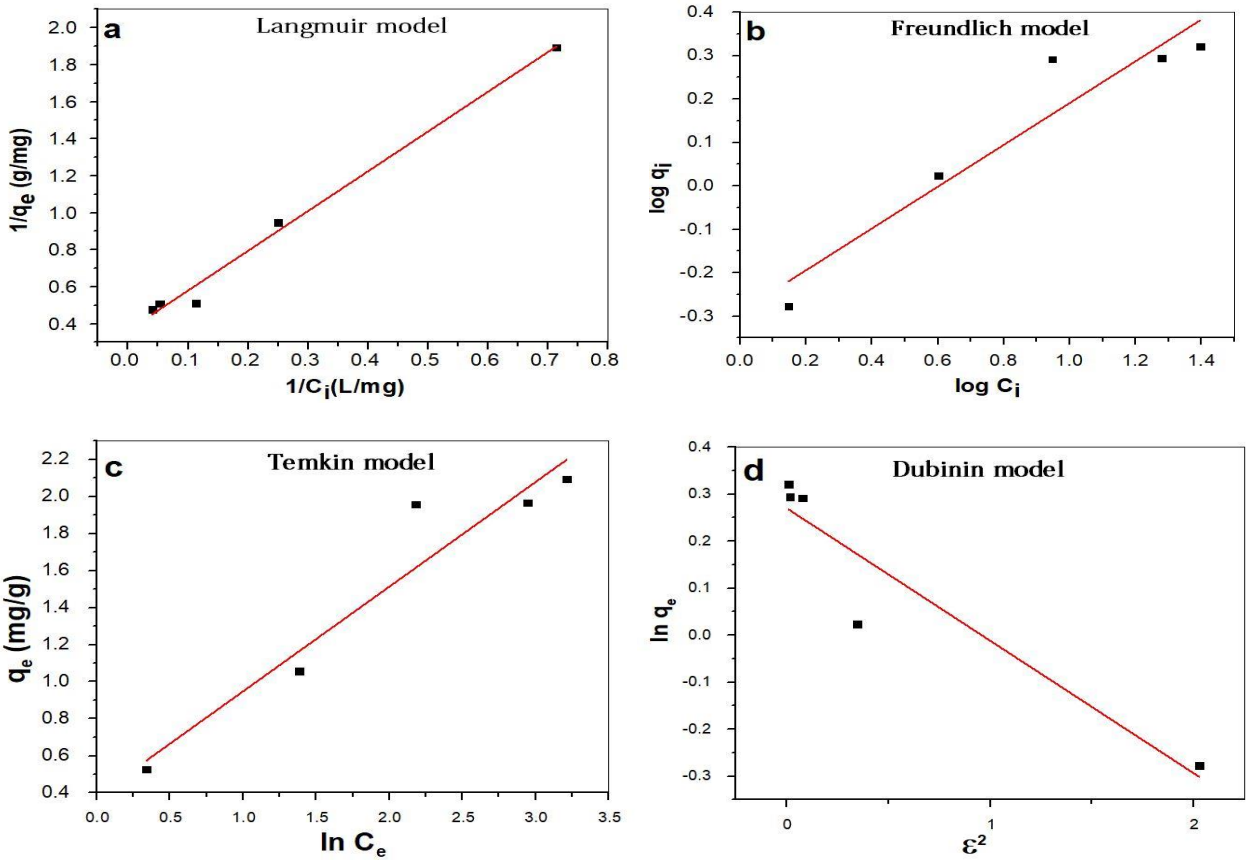

Figure 17. Isotherm models.

Table 2.Thermodynamic coefficients.

Coefficients	ΔG∘	ΔH∘	ΔS∘	Ea	A
	kJ/mol	KJ/mol	kJ/mol.K	KJ/mol	J/mol.K
Values	-1.895	30.5	0.10173	30.502	2.048×10^5

Table 3. Isotherm factors for the adsorption of AB210 by ZnF-NPs at various concentrations (AB210).

Langmuir			Freundlich			Temkin			Dubinin				
q_{max}	K_L	R^2	R_L	K_F	$\frac{1}{n}$	R^2	K_T	B_T	R^2	q_m	β	E	R^2
0.465	5.887	0.991	0.662	0.74	0.481	0.91	1.00	0.56	0.92	1.31	0.282	1.33	0.9

Conclusion

Green ZnF-NPs nanoparticles were effectively synthesized using a eucalyptus plant extract and a microwave-assisted green technique. The characterization results of ZnF-NPs show porous

Published Online First: September, 2024
https://doi.org/10.21123/bsj.2024.9359
P-ISSN: 2078-8665 - E-ISSN: 2411-7986
Baghdad Science Journal

nanoparticles a particle size of 32 nm and SSA of 42 m^2/g. Furthermore, the crystalline structure and presence of certain polyphenol groups were proven through XRD and FT-IR results. Applying ZnF-NPs in the photocatalytic process gives better removal efficiency than the adsorption process, and photocatalytic degradation occurs more quickly than adsorption. A 100% removal efficiency was achieved at 5 mg/L of AB210 and was entirely removed within 30 minutes at optimal pH of 7, UV-intensity 24 W/m^2, and temperature of 45 ℃. During the photocatalytic process, the removal efficiency was 74% through adsorption. According to the thermodynamic and kinetic study, adsorption process was physisorption, endothermic, and the pseudo-second-order model kinetic provided best fit. As a consequence, green synthesis is a recommended technique for increasing ZnF-NPs photocatalytic activity, which is needed to remove different organic pollutants from wastewater.

Acknowledgment

The authors are grateful to the Department of Biochemical Engineering, Al-Khwarizmi College of Engineering, and Nahrain University for providing facilities for the characterization of nanoparticles. The Environment and Water Directorate of Iraq's Ministry of Science and Technology for supplying all of the necessary resources.

Authors' Declaration

- Conflicts of Interest: None.
- We hereby confirm that all the Figures and Tables in the manuscript are ours. Furthermore, any Figures and images, that are not ours, have been included with the necessary permission for re-publication, which is attached to the manuscript.
- No animal studies are present in the manuscript.
- No human studies are present in the manuscript.
- No potentially identified images or data are present in the manuscript.
- Ethical Clearance: The project was approved by the local ethical committee at Ministry of Science and Technology.

Authors' Contribution Statement

A.K. H. designed the experiments and corrected the manuscript, M. A. A. supervised the work, critically revised the manuscript, and proved the manuscript and Z. A. N. collected the data, analyzed/interpreted the results, and drafted the manuscript.

References

1. Noormohamad HR, Mohammed AH, Ahmad M Bin. Kinetic Study of Polymerization Isopropylacrylamide in Aqueous Solution. Baghdad Sci J. 2023; 20(5): 1926-1932. https://doi.org/10.21123/bsj.2023.7523
2. Ali N, Zada A, Zahid M, Ismail A, Rafiq M, Riaz A, et al. Enhanced photodegradation of methylene blue with alkaline and transition-metal ferrite nanophotocatalysts under direct sun light irradiation. J Chin Chem Soc. 2018; 66(4) :1-7.https://doi.org/10.1002/jccs.201800213
3. Al-Qahtani KM, Cadmium removal from aqueous solution by green synthesis zero valent silver nanoparticles with Benjamina leaves extract, Egypt J Aquat Res. 2017; 43(6): 269–274. https://doi.org/10.1016/j.ejar.2017.10.003
4. Luaibi I M, Atiya MA, Hassan AK, Mahmoud ZA. Heterogeneous catalytic degradation of dye by Fenton-like oxidation over a continuous system based on Box–Behnken design and traditional batch experiments. Karbala Int J Mod Sci. 2022; 8(2): 9–28.https://doi.org/10.33640/2405-609x.3217
5. AlShaheeb ZA, Thabit ZA, Oraibi AG. Effect of Green-biosynthesis Aluminum Nanoparticles (Al NPs) on Salmonella enterica Isolated from Baghdad City. Baghdad Sci J. 2023; 20(5): 1840-1857. https://doi.org/10.21123/bsj.2023.7526
6. Vasantharaj S, Sathiyavimal S, Senthilkumar P, Kalpana VN, Rajalakshmi G, Alsehli M, et al. Enhanced photocatalytic degradation of water pollutants using bio-green synthesis of zinc oxide nanoparticles (ZnO NPs). J Environ Chem Eng. 2021; 9(4): 105772. https://doi.org/10.1016/j.jece.2021.105772
7. Abdi J, Vossoughi M, Mahmoodi NM, Alemzadeh I. Synthesis of metal-organic framework hybrid nanocomposites based on GO and CNT with high adsorption capacity for dye removal. Chem Eng J. 2017; 326(6): 1145-

Published Online First: September, 2024
https://doi.org/10.21123/bsj.2024.9359
P-ISSN: 2078-8665 - E-ISSN: 2411-7986
Baghdad Science Journal

1158.https://doi.org/10.1016/j.cej.2017.06.054
8. Liu Y, Zhang Q, Xu M, Yuan H, Chen Y, Zhanog J, et al. Novel and efficient synthesis of Ag-ZnO nanoparticles for the sunlight-induced photocatalytic degradation. Appl Surf Sci. 2019; 476(9): 632-640. https://doi.org/10.1016/j.apsusc.2019.01.137
9. Yadav N, Kola AK, Naz I, Saroj D. A review on advanced physico-chemical and biological textile dye wastewater treatment techniques. Rev Environ Sci Bio Technol. 2020; 19: 543–560.https://doi.org/10.1007/s11157-020-09543-z
10. Alkasir M, Samadi N, Sabouri Z, Mardani Z, Khatami M, Darroudi M. Evaluation cytotoxicity effects of biosynthesized zinc oxide nanoparticles using aqueous Linum Usitatissimum extract and investigation of their photocatalytic activityackn. Inorg Chem Commun. 2020; 119: 108066. https://doi.org/10.1016/j.inoche.2020.108066
11. Dheeb BI, Al-Dujayli S, Ibrahim IM, Abbas QA, Ali AH, Ramizy A, et al. Study the Antifungal Activity of ZnS:Mn Nanoparticles Against Some Isolated Pathogenic Fungi. J Phys Conf Ser. 2019; 7(1): 1178. https://doi.org/10.1088/1742-6596/1178/1/012008
12. Barzinjy AA, Azeez HH. Green synthesis and characterization of zinc oxide nanoparticles using Eucalyptus globulus Labill . leaf extract and zinc nitrate hexahydrate salt. SN Appl Sci. 2020; 2(5): 1-14. https://doi.org/10.1007/s42452-020-2813-1
13. Patel H. Fixed - bed column adsorption study : a comprehensive review. Appl Water Sci. 2020; 9(45): 349. https://doi.org/10.1007/s13201-019-0927-7
14. Nakate UT, Patil P, Nakate YT, Na S In, Yu YT, Hahn Y bong. Ultrathin ternary metal oxide Bi_2MoO_6 nanosheets for high performance asymmetric supercapacitor and gas sensor applications. Appl Surf Sci. 2021; 551(1): 149422. https://doi.org/10.1016/j.apsusc.2021.149422
15. Raizada P, Sudhaik A, Patial S, Hasija V, Khan AP, Singh P, et al. Engineering nanostructures of CuO-based photocatalysts for water treatment : Current progress and future challenges. Arab J Chem. 2020; 13(11): 8424-8457.https://doi.org/10.1016/j.arabjc.2020.06.031
16. Altıntıg E, Yenigun M, Sarı A, Altundag H, Tuzen M, Saleh TA. Facile synthesis of zinc oxide nanoparticles loaded activated carbon as an eco-friendly adsorbent for ultra-removal of malachite green from water. Environ Technol Innov. 2021; 21: 101305. https://doi.org/10.1016/j.eti.2020.101305
17. Atiya MA, Hassan AK, Luaibi IM. Green Synthesis Of Bimetallic Iron/Copper Nanoparticles Using Ficus Leaves Extract For Removing Orange G(OG) Dye From Aqueous Medium. Nat Env Poll Tech. 2022; 21(1): 355-365. https://doi.org/10.46488/NEPT.2022.v21i01.043
18. Atiya MA, Ridha MJ, Saheb MA. Removal of Aniline Blue from Textile Wastewater using Electrocoagulation with the Application of the Response Surface Approach. J Eng Sci Technol. 2020; 61(11): 2797-2811.https://doi.org/10.24996/ijs.2020.61.11.4
19. Ali J, Ali N, Wang L, Waseem H, Pan G. Revisiting the mechanistic pathways for bacterial mediated synthesis of noble metal nanoparticles. J Microbiol Methods. 2019; 159(2): 18-25.https://doi.org/10.1016/j.mimet.2019.02.010
20. Mahmoud ZA, Atyia MA, Hassan AK. The Influence of Support Materials on The Photo-Fenton-like Degradation of Azo Dye Using Continuous Nanoparticles Fixed-bed Column. Al-Khwarizmi Eng. 2022; 18(4): 14-31. https://doi.org/10.22153/kej.2022.09.002
21. Yaseen S, Yassen A, Ismail O, Yassin A. Sustainable fabrication, optical properties and rapid performance of bio-engineered copper nanoparticles in removal of toxic methylene blue dye in an aqueous medium. Curr Res Green Sustain Chemi. 2021; 4: 100103. https://doi.org/10.1016/j.crgsc.2021.100103
22. Kamli MR, Malik MA, Srivastava V, Sabir JSM, Mattar EH, Ahmad A. Biogenic zno nanoparticles synthesized from origanum vulgare abrogates quorum sensing and biofilm formation in opportunistic pathogen chromobacterium violaceum. Pharmaceutics. 2021; 13(11): 1743. https://doi.org/10.3390/pharmaceutics13111743
23. Ajormal F, Moradnia F, Taghavi S, Ramazani A. Zinc Ferrite Nanoparticles in Photo-Degradation of Dye : Mini-Review. J Chem Rev. 2020; 2(2): 90-102. https://doi.org/10.33945/SAMI/JCR.2020.2.2
24. Din MI, Jabbar S, Najeeb J, Khalid R, Ghaffar T, Arshad M K, et al. Green synthesis of zinc ferrite nanoparticles for photocatalysis of methylene blue. Int J Phytoremediation. 2020: 6(10): 1-8. https://doi.org/10.1080/15226514.2020.1781783
25. Makofane A, Motaung DE, Hintsho-mbita NC. Photocatalytic degradation of methylene blue and sulfisoxazole from water using biosynthesized zinc ferrite nanoparticles. Ceram Int. 2021; 2(4): 0272-8842. https://doi.org/10.1016/j.ceramint.2021.04.274
26. Madhukara Naik M, Bhojya Naik HS, Nagaraju G, Vinuth M, Raja Naika H, Vinu K. Green synthesis of zinc ferrite nanoparticles in Limonia acidissima juice: Characterization and their application as photocatalytic and antibacterial activities. Microchem J. 2019; 146: 1227-1235. https://doi.org/10.1016/j.microc.2019.02.059
27. Hassan AK, Atiya MA, Mahmoud ZA. Photo-Fenton-like degradation of direct blue 15 using fixed bed reactor containing bimetallic nanoparticles: Effects and Box–Behnken optimization. Environ Technol Innov. 2022; 28: 102907.https://doi.org/10.1016/j.eti.2022.102907
28. Abril D, Ferrer V, Mirabal-Gallardo Y, Cabrera-Bajas G, Segura C, Marican A, et al. Comparative Study of Three Dyes Adsorption onto Activated Carbon from Chenopodium quinoa Willd and

Published Online First: September, 2024
https://doi.org/10.21123/bsj.2024.9359
P-ISSN: 2078-8665 - E-ISSN: 2411-7986
Baghdad Science Journal

Quillaja saponaria. Mater. 2022; 15(14): 4898. https://doi.org/10.3390/ma15144898
29. Atiya MA, Mahmoud ZA, Hassan AK. Fenton-like degradation of direct blue dye using green synthesised Fe / Cu bimetallic nanoparticles. J Environ Eng Sci. 2022; 2(9): 1-16.https://doi.org/10.1680/jenes.22.00025
30. Aziz EK, Abdelmajid R, Rachid LM, Haddad E. Adsorptive removal of anionic dye from aqueous solutions using powdered and calcined vegetables wastes as low-cost adsorbent. Arab J Basic Appl Sci. 2018; 25(1): 1-10. https://doi.org/10.1080/25765299.2018.1517861
31. Surendra BS, Nagaswarupa HP, Hemashree MU, Khanum J. Jatropha extract mediated synthesis of $ZnFe_2O_4$ nanopowder: Excellent performance as an electrochemical sensor, UV photocatalyst and an antibacterial activity. Chem Phys Lett. 2019; 739(2): 136980.https://doi.org/10.1016/j.cplett.2019.136980
32. Bora L V, Mewada RK. Visible/solar light active photocatalysts for organic effluent treatment: Fundamentals, mechanisms and parametric review. Renew Sustain Energy Rev. 2017; 76: 1393-1421. https://doi.org/10.1016/j.rser.2017.01.130
33. Park J.K, Pupa EJ, Arif MH, Li JF, Anandapadmanaban G, Kang JP, et al. Synthesis of zinc oxide nanoparticles from Gynostemma pentaphyllum extracts and assessment of photocatalytic properties through malachite green dye decolorization under UV illumination-A Green Approach. Optik. 2021; 239(8): 166249.https://doi.org/10.1016/j.ijleo.2020.166249
34. Yagub MT, Sen TK, Afroze S, Ang HM. NU SC. Adsorptive removal of methyl orange dye from aqueous solution using populous leaves: Insights from kinetics, thermodynamics and computational studies. Adv Colloid Interface Sci. 2014; 3(7): 172-181. https://doi.org/10.1016/j.cis.2014.04.002
35. Akhtar MJ, Alhadlaq HA, Alshamsan A, Khan MAM, Ahamed M. Aluminum doping tunes band gap energy level as well as oxidative stress-mediated cytotoxicity of ZnO nanoparticles in MCF-7 cells. Nat Publ Gr. 2015; 1(9): 1-16. https://doi.org/10.1038/srep13876
36. Khan MS, Dhavan PP, Jadhav BL, Shimpi NG. Ultrasound-Assisted Green Synthesis of Ag-Decorated ZnO Nanoparticles UsingExcoecaria agallochaLeaf Extract and Evaluation of Their Photocatalytic and Biological Activity. Chemi Eur J. 2020; 41(5): 12660-12671.https://doi.org/10.1002/slct.202002905
37. Puthukkara P AR, Jose T S, lal S D. Plant mediated synthesis of zero valent iron nanoparticles and its application in water treatment. J Environ Chem Eng. 2021; 9(1): 104569. https://doi.org/10.1016/j.jece.2020.104569
38. Raghav S, Kumar D. Adsorption Equilibrium, Kinetics, and Thermodynamic Studies of Fluoride Adsorbed by Tetrametallic Oxide Adsorbent. J Chem Eng Data. 2018; 63(5): 1682-1697. https://doi.org/10.1021/acs.jced.8b00024
39. Ranjith E, Jayaprakash R, Seehra MS, Prakash T, Kumar S. Effect of a -Fe_2O_3 phase on structural , magnetic and dielectric properties of Mn – Zn ferrite nanoparticles. J Phys Chem Solids. 2013; 74(7): 943-949. https://doi.org/10.1016/j.jpcs.2013.02.013
40. Selvaraj R, Pai S, Murugesan SP, Pandey S, Bhole R, Gonsalves D, et al. Green synthesis of magnetic a-Fe_2O_3 nanospheres using Bridelia retusa leaf extract for Fenton-like degradation of crystal violet dye. Appl Nanosci. 2021; 11(8): 2227–2234https://doi.org/10.1007/s13204-021-01952-y
41. Chen L, Tian J, Qiu H, Yin Y, Wang X, Dai J, et al. Preparation of TiO_2 nanofilm via sol-gel process and its photocatalytic activity for degradation of methyl orange. Ceram Int. 2009; 35(8): 3275-3280. https://doi.org/10.1016/j.ceramint.2009.05.021
42. Lara M, Hussein A, Nguyen VQ, Kumar DR, Sayed MS, Tuma D, et al. Eco-friendly synthesis of recyclable mesoporous zinc ferrite @ reduced graphene oxide nanocomposite for efficient photocatalytic dye degradation under solar radiation. J Colloid Interface Sci. 2019; 1(5): 459-469. https://doi.org/10.1016/j.jcis.2019.11.018
43. Azizi S, Shahri MM, Mohamad R. Green synthesis of zinc oxide nanoparticles for enhanced adsorption of lead Ions from aqueous solutions: Equilibrium, kinetic and thermodynamic studies. Molecules. 2017; 22(6): 831. https://doi.org/10.3390/molecules22060831
44. Saleh TA, Al-Ruwayshid SH, Sarı A, Tuzen M. Synthesis of silica nanoparticles grafted with copolymer of acrylic acrylamide for ultra-removal of methylene blue from aquatic solutions. Eur Polym J. 2020; 130(4): 109698. https://doi.org/10.1016/j.eurpolymj.2020.109698
45. Zafar MN, Dar Q, Nawaz F, Zafar MN, Iqbal M, Nazar MF. Effective adsorptive removal of azo dyes over spherical ZnO nanoparticles. J Mater Res Technol. 2019; 8(1): 713-725. https://doi.org/10.1016/j.jmrt.2018.06.002
46. Tuzen M, Sarı A, Saleh TA. Response surface optimization, kinetic and thermodynamic studies for effective removal of rhodamine B by magnetic AC/CeO_2 nanocomposite. J Environ Manage. 2018; 206: 170-177. https://doi.org/10.1016/j.jenvman.2017.10.016
47. Liu X, Ye L, Liu S, Li Y, Ji X. Photocatalytic reduction of CO_2 by ZnO micro/nanomaterials with different morphologies and ratios of {0001} facets. Sci Rep. 2016; 6(5): 1-9. https://doi.org/10.1038/srep38474
48. Xiang H, Ren G, Zhong Y, Xu D, Zhang Z, Wang X, et al. Fe_3O_4 @ C Nanoparticles Synthesized by In Situ Solid-Phase Method for Removal of Methylene Blue.

Published Online First: September, 2024
https://doi.org/10.21123/bsj.2024.9359
P-ISSN: 2078-8665 - E-ISSN: 2411-7986
Baghdad Science Journal

Nanomater. 2021; 11(2): 330. https://doi.org/10.3390/nano11020330
49. Weldegebrieal GK. Synthesis method, antibacterial and photocatalytic activity of ZnO nanoparticles for azo dyes in wastewater treatment: A review. Inorg Chem Commun. 2020; 120(6): 108140. https://doi.org/10.1016/j.inoche.2020.108140
50. Ullah, R, Shah S, Muhammad Z, Shah AS, Faisal S, Khattak U, et al. In vitro and in vivo applications of Euphorbia wallichii shoot extract-mediated gold nanospheres. Green Process Synth. 2021; 10(1): 101–111. https://doi.org/10.1515/gps-2021-0013
51. Kainat, Khan MA, Ali F, Faisal S, Rizwan M, Hussain Z, et al. Exploring the therapeutic potential of Hibiscus rosa sinensis synthesized cobalt oxide (Co_3O_4-NPs) and magnesium oxide nanoparticles (MgO-NPs). Saudi J Biol Sci. 2021; 28(9): 5157-5167. https://doi.org/10.1016/j.sjbs.2021.05.035
52. Sonal S, Mishra B K. Role of hybrid systems and their importance in the dye degradation : trend and future aspect. Elsevier, 2021; 4(2) :545–571. https://doi.org/10.1016/b978-0-12-823876-9.00002-0
53. Romdhane DF, Satlaoui Y, Nasraoui R, Charef A, Azouzi R. Adsorption, Modeling, Thermodynamic, and Kinetic Studies of Methyl Red Removal from Textile-Polluted Water Using Natural and Purified Organic Matter Rich Clays as Low-Cost Adsorbent. J Chem. 2020; 7(5): 2020. https://doi.org/10.1155/2020/4376173
54. Haryono H, Ishmayana S, Fauziyah I. Synthesis and Characterization of Calcium Oxide Impregnated on Silica from Duck Egg Shells and Rice Husks as Heterogeneous Catalysts for Biodiesel Synthesis. Baghdad Sci J. 2023; 20(5): 1976-1984. https://doi.org/10.21123/bsj.2023.7895

الامتزاز والتحفيز الضوئي للتخليق الحيوي لجسيمات الزنك الفريت النانوية لإزالة الصبغة الحمضية السوداء 210 من الوسط المائي

زهراء عقيل نجم[1]، محمد عبد عطيه[1]، أحمد خضير حسان[2]

[1]قسم هندسة الكيمياء الاحيائية ،كلية الهندسة الخوارزمي، جامعة بغداد، بغداد، العراق
[2]مركز بحوث البيئة والمياه، وزارة العلوم والتكنولوجيا، بغداد، العراق

الخلاصة

عالجت هذه الدراسة مياه الصرف الصحي الملوثة بصبغة حمض الأسود 210 عن طريق تقنية الامتزاز والتحفيز الضوئي باستخدام جزيئات الزنك الفريت النانوية. تم تشكيل جسيمات الزنك الفريت النانوية بتقنية التخليق الأخضر باستخدام أوراق الأوكالبتوس كعامل اختزال. المسح المجهري للإلكترون ، الأشعة السينية المشتتة للطاقة ، حيود الأشعة السينية ، Brunauer-emmett -teller، مقياس زيتا. أشارت الصور من SEM إلى التبلور والشكل الكروي للجسيمات النانوية المصنوعة من الفريت الزنك بحجم جسيم يبلغ 32 نانومتر. بالإضافة إلى ذلك ، تضمنت هذه الدراسة استخدام مفاعل ضوئي لإنجاز عملية التحلل الضوئي. تم فحص تأثير العوامل الرئيسية على الامتزاز و التحلل الضوئي للصبغة. بناءً على نتائج الامتزاز ، كانت فعالية إزالة الصبغة بعد 180 دقيقة 74٪ في الظروف المثلى 5 غم / لتر ، 0.75 غم / لتر ، 5 ، 45 درجة مئوية لتركيز AB210 ، جرعة الجسيمات النانوية الفريت الزنك ، ودرجة الحموضة ، ودرجة الحرارة ، على التوالي. في المقابل ، أظهرت نتائج التحلل الضوئي أنه تمت إزالة خمسة ملغم / لتر من الصبغة بالكامل في غضون 30 دقيقة عند درجة الحموضة المثلى 7 ، وشدة الأشعة فوق البنفسجية 24 واط / م^2 ، ودرجة حرارة 45 درجة مئوية. تمت دراسة متساوي درجة حرارة الامتزاز باستخدام نماذج Freundlich و Langmuir و Temkin و Dubinin .

الكلمات المفتاحية: عملية الامتزاز، الطريقة الخضراء، الدراسات الحركية والحرارية الديناميكية، المحفز الضوئي، جسيمات نانوية من فيريت الزنك.